The extragalactic heritage of the Layer-Oriented MAD at VLT

Renato Falomo[1a] and Roberto Ragazzoni[1]

INAF - Osservatorio Astronomico di Padova, Italy

Abstract. The layer-oriented wavefront sensor onboard MAD, capable to catch up to 8 stars on the pins of pyramids in a 2 arcmin Field of View has been tested at the VLT in a unique dedicated run lasting 6 consecutive nights. As this kind of MCAO observations is focused onto a field with many relatively faint reference stars our main focus was onto extragalactic targets that are plagued by the problem of limited sky coverage. While we achieved demonstrative science onto a very crowded field using a globular cluster, allowing to assess firmly the compensation stability over the FoV,we succeeded into securing scientific data for a number of extragalctic sources from the local Universe up to z ∼ 3. In particular we devised stellar population study in a dwarf galaxy, morphology of the jets in nearby AGN and the properties of the environment for high redshift quasars. The scientific outcome of the observation run, consisting into 6 published refereed papers and two forthcoming, is briefly reported along with some lessons learned.

1 Introduction

MAD is a project [20] mainly developed by ESO to test the Multi Conjugated Adaptive Optics (MCAO) capabilities on the sky, in the framework of the design of an Extremely Large Telescope (ELT). The instrument was mounted on the UT-3 of VLT to realize the first MCAO observation on sky [1]. It accommodates two wavefront sensors (WFS): a Star Oriented multi Shack–Hartmann and a Layer Oriented [28,36] multi pyramid [27]. Both WFS can use reference stars on a 2 arcmin technical FoV. MAD is complemented with the CAMCAO scientific IR camera, with a $2k \times 2k$ Hawaii II IR detector that can be moved across the 2 arcmin corrected circular FoV. The pixel scale is 0.028 arcsec/pixel, yielding a 57 arcsec × 57 arcsec square FoV on the detector.

2 Resolved stellar population

The study of the resolved stellar populations in external galaxies has greatly developed in the last decade, to become arguably the most accurate tool to investigate the star formation history in stellar systems. However, due to the severe crowding of stars, with standard instrumentation at ground based telescopes this study is limited to the nearest galaxies. High precision photometry for the most distant galaxies in the Local Group (LG) and beyond can be obtained only with the HST.

The near-infrared (IR) colour-magnitude diagrams clearly show the sequences of Asymptotic Giant Branch (AGB) stars, red supergiants, and red giant branch (RGB) stars down to ∼1 mag below the RGB tip. Optical–near-IR diagrams, obtained by combining our data with WFPC2 observations, provide the best separation of stars in the various evolutionary stages. The counts of AGB stars brighter than the RGB tip allow us to estimate the star formation at intermediate ages. Assuming a Salpeter initial mass function, we find that the star formation episode at intermediate ages produced $\sim 5 \times 10^5\ M_\odot$ of stars in the observed region.

In order to study the stellar content from CMD of resolved stellar population we obtained near-infrared (IR) images of the dwarf irregular galaxy UKS 2323-326[12]. This galaxy was chosen from a list of targets selected according to various criteria: favorable position on the sky with respect to the availability of stars to perform the AO correction; low Galactic latitude, to minimize the contamination by foreground Galactic stars; location slightly beyond the boundary of the LG, so as to maximize the physical area sampled within the 1 arcmin field-of-view (FoV) while still detecting stars at the Tip of

[a] renato.falomo@oapd.inaf.it

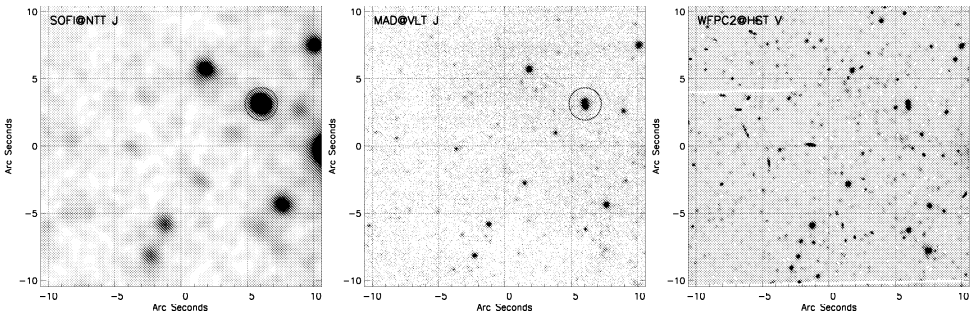

Fig. 1. SOFI, MAD and WFPC2 images of the same region in UKS 2323-326. Only a section of the full area analyzed in our study is shown to better illustrate the details. The two circles highlight the effect of the higher spatial resolution of MAD versus SOFI. (see [12])

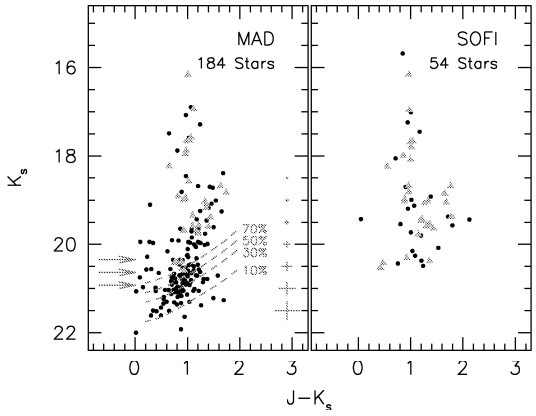

Fig. 2. CMD obtained from MAD data (*left*) and from SOFI data (*right*) for the same FoV (see [12] for details). In the left panel the completeness levels *dashed lines* and photometric errors *crosses* from artificial star experiments are shown. The expected location of the TRGB is indicated with arrows for [Fe/H] = −1.0, −1.5 and −2.0 (top to bottom). Stars used as secondary photometric standards are shown as triangles.

the Red Giant Branch (TRGB) with an adequate S/N; existence of images of the same field in HST and/ or ESO archives; the presence of a relatively strong intermediate age component.

In Figure 1 we show the comparison of the observed field (by MAD) with that obtained with SOFI and with HST. These observations can be used to derive a rough estimate of the star formation occurred in UKS 2323-326 at intermediate ages by considering the number of AGB stars brighter than the TRGB, which is proportional to the gas mass converted into stars between $\sim$ 0.1 and a few Gyrs [10]. We constructed NIR CMD (see Fig. 2) that allows us to derive an accurate census of the bright evolved stellar population (red supergiants and AGB stars). The stellar distribution in our CMD is suggestive of an extended episode of star formation; by averaging our empirical calibration we obtain a specific production of 0.15 or 0.08 stars per $10^3 M_{\odot}$, if this episode started 1.5 or 3 Gyr ago respectively. In particular, this CMD shows also that all stars in the red tail, are located in the position expected for C-stars, since they are compatible with the main locus of C-star in nearby dwarf galaxies.

3 The jet of BL Lacertae objects

BL Lac objects are a class of low–power active galactic nuclei (AGN) characterized by a lack or extreme weakness of emission lines observed in all other types of AGN. They also exhibit strong and rapid flux variability and significant polarization. The emission is dominated by a non–thermal component extending from radio to very high energies. These active nuclei are hosted by massive

elliptical galaxies that appear in most cases unperturbed and located in moderately rich environments. A widely accepted model that explains these properties is based on the idea that these nuclei emit a relativistic jet oriented close to the line of sight of the observer.

Since the jet is closely aligned with the line of sight, it is very difficult to observe unless the angular resolution is high. In the radio band, jet detection is indeed possible and a large fraction of objects classified as BL Lacs show a signature of a jet, often with evidence of superluminal motion [23,11]. On the other hand, the jet is rarely detected in the optical and X-ray bands. This depends both on the more limited angular resolution and on the short lifetime of the high energy electrons producing the non–thermal emission of the jet.

Strong evidence of a prominent optical jet in a BL Lac object has been found for PKS 0521-365. This is a well-studied nearby object (z=0.0554) [2] and it is one of the most remarkable extragalactic objects of the southern sky (see [2,13,6,19,32]). Its optical spectrum shows the strong narrow and broad emission lines typical of type 1 active nuclei both in optical and UV [34,3,31]. The optical jet was observed with HST by [19,32], who found a structure consisting of a bright knot close to the nucleus and a diffuse and knotty structure that extends out to ∼ 6 arcsec from the nucleus. Farther out along the jet (but well separated), at ∼ 9 arcsec, there is resolved compact emission (also called the "red tip") [6,32].

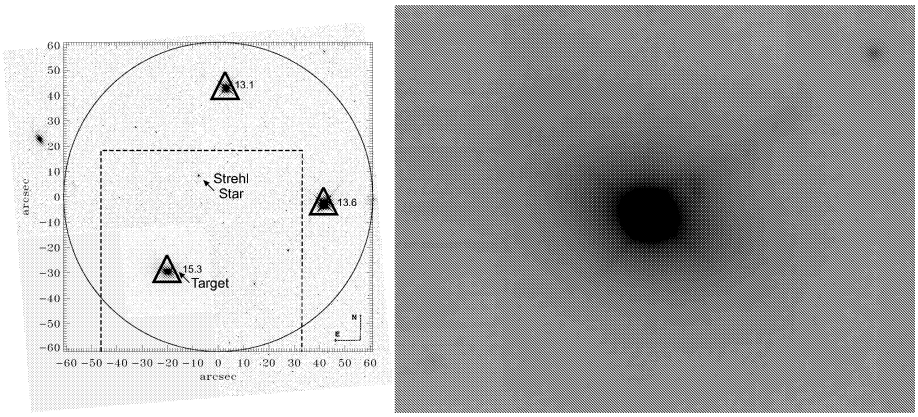

Fig. 3. *Left:* The 2 arcmin field of view (circle) corrected by the MAD MCAO system. The area inside the dashed box was imaged by the NIR camera. The grey scale image is a mosaic of HST + WFPC2 images (F702w filter). The triangles correspond to the LO AO reference stars. R-magnitude is reported for each star. At the centre of the field the arrow identifies the star used to compute the SR. *Right:* The MAD image of the target (PKS 0521-365) in K band.

The images were obtained in MCAO configuration with both the deformable mirrors and used two reference stars (R-band magnitudes: 13.6, 13.0) and the core of the target (R = 15.3) to perform wavefront sensing (see Figure 3).These correspond to an overall integrated magnitude of R ∼ 12.5. Given that MAD Wavefront Sensing CCD sensitivity is peaked in the V band we estimate an overall V ∼ 12 integrated magnitude using available colours of stars from USNO.

To enhance the structure of the jet in the near-IR image, we have subtracted the emission of both the nucleus and the host galaxy from the original image (see [5,9] for details). The emission from the jet after the subtraction of the nucleus and the host galaxy is shown in Fig. 4. The bright knot A at 1.9 arcsec from the nucleus and the diffuse emission from the jet are clearly detected in near-IR as well as the resolved feature in the red-tip.

To compare the features in NIR, optical, and radio bands, we applied the same procedure used for the MAD image to subtract the host galaxy and the nucleus from the HST R band image. In Fig. 5 we compare images of the jet in the three different bands. The overall morphology of the jet in the near-IR is similar to that observed in the optical [33] and at 2cm [13]. The general shape and total length of the radio jet are almost exactly reproduced in the near-IR, in the optical, and at radio frequencies.

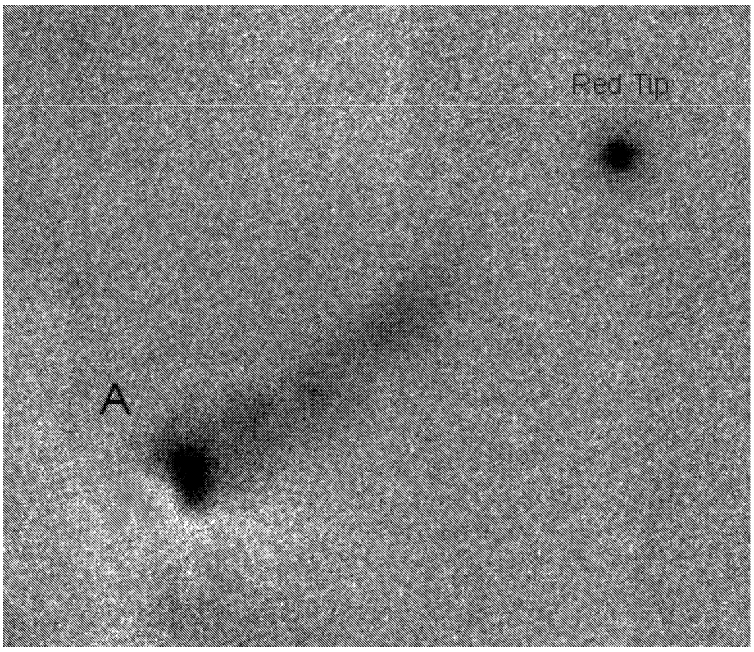

Fig. 4. The near-IR image of the jet of the BL Lac object PKS 0521-365, as observed by MAD at VLT in Ks filter. The host galaxy and the nucleus have been subtracted from the original image (see text). The field of view shown is 10 arcsec.

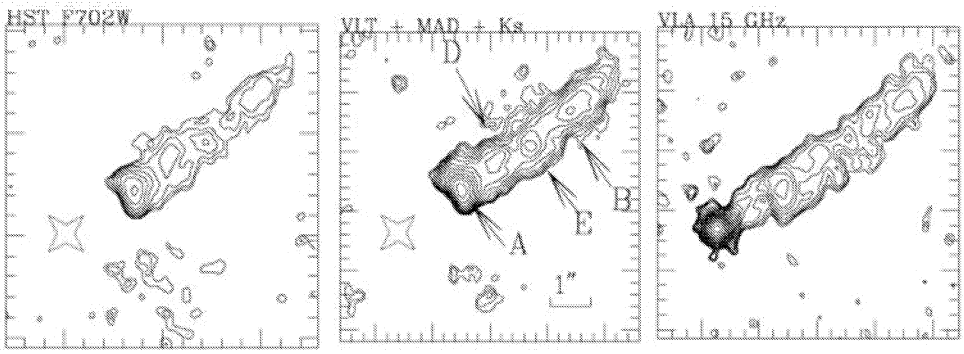

Fig. 5. The contour plot of the jet of PKS 0521–365 observed by MAD in the Ks band (middle panel) compared with the image of the jet observed in R band by HST+ WFPC2 (left panel) and the radio map at 15 GHz obtained by VLA (right panel). The large star represents the position of the (subtracted) nucleus in both optical and near-IR bands. In the right panel, the radio jet is shown at the same angular resolution as the near-IR data. The nuclear source has not been subtracted. A collimated jet with the same position angle as the VLBI pc-scale jet is present near the core. The jet becomes resolved transversally at less than 1" from the core.

Four knots can be easily recognized and have been labelled in Fig. 5, as in [6]. To construct the spectral emission of these components of the jet, we measured the flux of the four knots by adopting a fixed square aperture of 1 arcsec. We combined our near-IR measurements of the nucleus, jet knots, and hotspot with the available optical, radio and X-ray fluxes to construct overall spectral energy distributions (SED) of main components.

For the jet knots and hotspot, which are resolved in the radio, optical and near-IR images, we assume an emission region radius of 0.5 kpc. Since we do not detect any evidence of an inverse

Compton component in the X-ray emission of knot A and hotspot, we have determined the magnetic field imposing that the inverse Compton luminosity is lower than 10% of the synchrotron luminosity. The electron density is much lower than that in the nucleus which is consistent with the presumably more rarefied medium in the external regions of the jet with respect to the core (see also [9]).

4 Quasar host galaxies

In recent years it has become clear that super massive black holes (SMBH) are ubiquitous in nearby galaxies. The black hole masses are correlated with the properties of the surrounding galaxy bulge, namely luminosity or mass (via velocity dispersion). The cosmic history of black hole growth also appears to trace the cosmic star- formation rate, at least from redshift 0 to z ~ 1-2, establishing another connection between black hole and galaxy properties. These discoveries have changed our view of active galactic nuclei (AGN).

Accretion onto a central black hole now appears to be a common phase in the evolution of normal galaxies. Furthermore, SMBH may well have a period of maximum growth (maximum nuclear luminosity) contemporaneous with the bulk of the initial star formation in the bulge. This has led to a renewed interest in AGN properties, especially regarding the host galaxies. Studies of the co-evolution of SMBH and their host spheroids are obviously critical to understanding how and when galaxies in the local Universe formed and evolved.

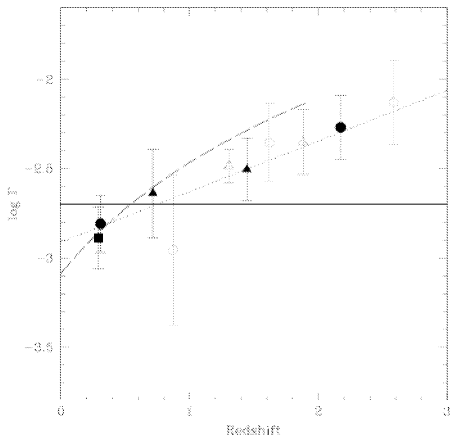

Fig. 6. The average values of Γ for the quasars [4] (filled symbols), together with the linear best fit (dotted line). Also shown [22] (dashed line). The average Γ values of the 51 lensed and non-lensed quasars from [25,26] (empty circles) and of the 89 AGN from [21] (empty triangles). The horizontal solid line represents the constant $\Gamma = 0.002$ case (reproduced from [4])

Direct measurements of $\mathcal{M}_{\rm BH}$ from gaseous or stellar dynamics require observations capable to resolve the BH sphere of influence, which are feasible only for a limited number of nearby galaxies. Therefore the only way to measure $\mathcal{M}_{\rm BH}$ in distant (>few tens of Mpc) galaxies is to focus on Type-1 AGNs, where $\mathcal{M}_{\rm BH}$ can be inferred from the width of emission lines Doppler-broadened by the BH potential well and from the AGN continuum luminosity [35], assuming the virial equilibrium. Quasars represent therefore the best tool to probe $\mathcal{M}_{\rm BH}$ at high redshift, thanks to their huge luminosity. Preliminary studies suggest that, for a given galaxy mass, black holes in high-z AGNs are more massive than their low-z counter-parts [22],[25],[26]. In Figure 6 we show the comparison of the evolution of the radio $\Gamma = \mathcal{M}_{\rm BH} / \mathcal{M}_{\rm host}$ from various sources (see [4]) All together these data depict an increase of Γ with z (see Fig 6).

The last ten years have yielded considerable progress in characterizing AGN host galaxies. Observationally, one needs excellent spatial resolution and a stable point spread function, in order to

minimize the contamination of the weak host galaxy nebulosity by the strong central point source. One also needs the largest possible telescope throughput to detect the low surface brightness emission at large galaxy radii. At low redshifts a major contribution to our knowledge of active nuclei host galaxies has been provided by images from the Hubble Space Telescope (HST).

At higher redshift (z >1) HST observations have been complemented by significant contributions from 8-m class ground- based telescopes under superb seeing conditions. Nevertheless even under exceptional seeing condition the presence of the luminous nucleus hinder the possibility to properly resolve and characterize the host properties in particular for luminous QSOs and relatively faint host galaxies.

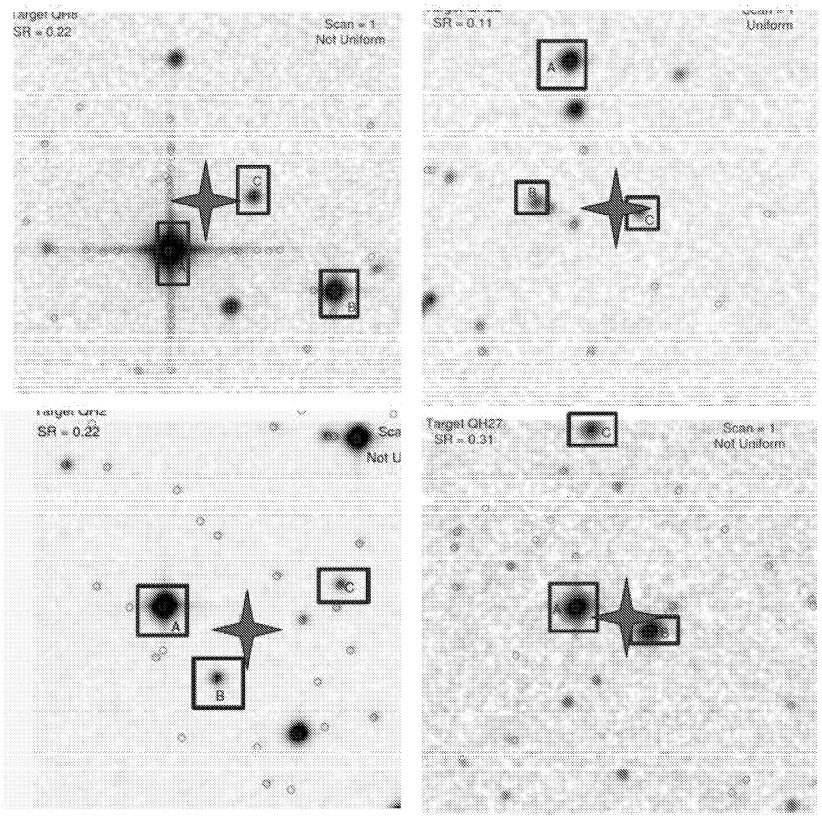

Fig. 7. Examples of high redshift quasars that can be observed with MCAO using a number of faint reference guide stars (inside the boxes) in a field of view of 2 arcmin. The red star represents the position of the target.

On the other hand to understand the coevolution of SMBH and their hosting galaxies it is of fundamental relevance to characterize the properties of QSO host galaxies at high redshift. Till now only few objects have been resolved at high z ([7,25,14,8,15]) because of the lack of suitable instrumentation. The use of adaptive optics is probably the best technique that is able to combine narrow PSF (to suppress the light from the nucleus) and large collecting power (needed to detect the faint surface brightness of distant galaxies). Unfortunately this kind of observations can be performed only for targets that are close to bright reference guide stars and because of the low surface density of QSOs only few objects can be observed with standard (SCAO) adaptive optics. This limit is expected to change with AO that uses either Laser Guide Stars (artificial reference guide star) or with MCAO systems and natural guide stars (enlargement of the usable field of view). Example for the latter is MAD experiments that, in addition to a much more uniform PSF over the field can improve the sky coverage of

QSO candidates also because of the use of pyramid LO WFS. In this case in fact we require that the total flux of a number of stars around the target is above a given threshold instead of the flux of an individual AO star.

Examples of high redshift QSO with a number of faint AO stars is shown in Figure 7. These objects can not be observed with standard SCAO since the individual stars around the targets are too faint.

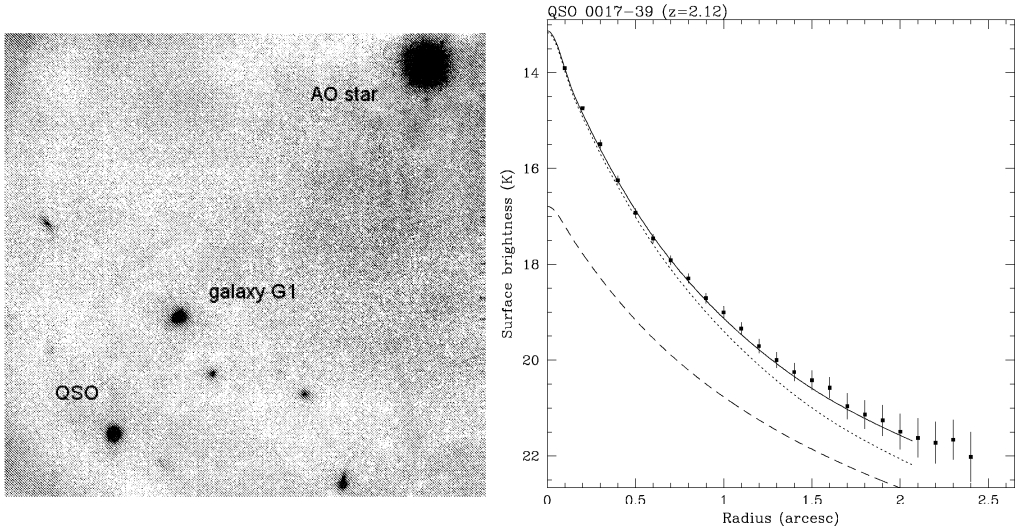

Fig. 8. *Left:* The image obtained with MAD (K band) of the QSO 0017-3916 (z=2.12) *Right:* The radial brightness profile of the QSO (filled squares) is decomposed into the nucleus (described by the PSF; dotted line) and the host galaxy (modeled by a Sersic law; dashed line). Best fit (solid line).

During the observing run with MAD we obtained images of a number of high redshift quasars under average seeing conditions. As example of characterization of a luminous high z QSO host we show here the case of Q0017-3916 (z = 2.12) (see Figure 8). This K band image was obtained under 0.85 arcsec seeing condition and using three reference guide stars. The final image was obtained from the combination of 75 individual frames and the resulting quality yields FWHM of 0.16 arcsec and an encircled energy of 50% at radius of 0.27 arcsec (radius = 0.95 arcsec at 90% EE). The QSO is well resolved (see Figure 8) and the 2D fit assuming the PSF derived by the reference star in the field yields a galaxy with K = 17.5 (corresponding to M(R) = - 24.4 (assuming 3.1 mag of k-correction and filter transformation), effective radius of 0.8 arcsec (corresponding to 4 kpc at z = 2.12).

5 Conclusions

We have presented MCAO near-IR observations of some extragalactic sources obtained with MAD@VLT. These results underline the powerful capabilities of MCAO data for various types of extragalactic objects. The limits in terms of magnitude limits for the AO reference stars are related to the efficiency of the equipment used in the experiment and to the 8m aperture of VLT. These limits are expected to be greatly surpassed by the use of similar devices in ELTs. This would also provide a much larger sky covering using natural guide stars and pyramid WFS.

6 Acknowledgments

We are grateful to all our collaborators that have been involved in the MAD experiment and in particular to those that contributed to the results reported here: C. Arcidiacono,J. Farinato, G. Giovannini, L.Greggio, Gullieuszik, M., E. Liuzzo, E. Marchetti, A. Moretti, E. Pian and A. Treves.

References

1. Bouy, H., Kolb, J., Marchetti, E., et al. 2008, A&A, 477, 681
2. Danziger I.J., Fosbury R.A.E., Goss W.M. & Ekers R.D. 1979 MNRAS 188, 415
3. Danziger, I.J., Bergeron, J., Fosbury, R. A. E. et al1983 MNRAS 203 565
4. Decarli, R. Falomo, R. Treves, A., Kotilainen, J., Labita M. and Scarpa, R. 2009 MNRAS **402** 2453
5. Falomo, R. , Scarpa R., Treves, A. and Urry, 2000, Ap.J, 542, 731
6. Falomo R. 1994 The Messenger 77, 49
7. Falomo R., Kotilainen J.K., Scarpa R., Treves A., 2005, A&A, 434, 469
8. Falomo R., Treves A., Kotilainen J.K., Scarpa R., Uslenghi M., 2008, ApJ, 673, 694
9. Falomo, R., Pian, E. Treves, A., Giovannini, G. Venturi, T., et al 2009 A&A 501 907
10. Greggio L. ASP Conf. Ser 274 (2002) 444
11. Giroletti, M., Giovannini, G., Taylor, G.B., & Falomo, R. 2004, ApJ, 613, 752
12. Gullieuszik, M. Greggio, L. Held, E.V. Moretti, et al 2008 A&A 483 L5
13. Keel, W.C. 1986, ApJ, 302, 296
14. Kotilainen J.K., Falomo R., Labita M., Treves A., & Uslenghi M., 2007, ApJ 660 1039
15. Kotilainen J.K., Falomo R., Decarli R., Treves A., Uslenghi M., Scarpa R., 2009, ApJ 703 1663.
16. Labita M., Decarli R., Treves A., Falomo R., 2009a, MNRAS, 396, 1537
17. Labita M., Decarli R., Treves A., Falomo R., 2009b, MNRAS , 339 2099.
18. Liuzzo, E. Falomo, R., Treves, A., Donato, D, Sambruna, R. et al 2011 A&A 528 34
19. Macchetto F., Albrecht R., Barbieri C., et al 1991 ApJ 369, L55
20. Marchetti, E., Brast, R., Delabre, B., et al. 2007, The Messenger, 129, 8
21. Merloni A., Bongiorno A., Bolzonella M., et al., 2010, ApJ 708 137.
22. McLure R.J., Jarvis M.J., Targett T.A., Dunlop J.S., Best P.N., 2006, MNRAS, 368, 1395
23. Homan, D.C., Ojhia, R., Wardle, J.F.C., et al., 2001, ApJ, 549, 840
24. Peng,C.Y., Impey,C.D., Rix,H.-W., et al. 2006, ApJ, 649, 616
25. Peng C.Y., Impey C.D., Ho L.C., Barton E.J., Rix H.-W., 2006a, ApJ, 640, 114
26. Peng C.Y., Impey C.D., Rix H.-W., Kochanek C.S., Keeton C.R. et al 2006b, ApJ, 649, 616
27. Ragazzoni, R. 1996, Journal of Modern Optics, 43, 289
28. Ragazzoni, R., Farinato, J., & Marchetti, E. 2000, in Proc. SPIE, Vol. 4007, Adaptive Optical Systems Technology, ed. P. L. Wizinowich, 1076
29. Shen Y., Greene J.E., Strauss M.A., Richards G.T., Schneider D.P., 2008, ApJ, 680, 169
30. Sparks W.B., Biretta J.A. & Macchetto F. 1994 ApJS 90, 909
31. Scarpa R., Falomo R. & Pian E. 1995 AA 303, 730
32. Scarpa, R., Urry, C.M., Falomo, R., & Treves, A. 1999, ApJ, 526, 643
33. Scarpa R., Urry C.M., Falomo R, Pesce J.E., Giavalisco M. & Treves A. 2000 ApJ 532, 740.
34. Ulrich M.E. 1981, AA 103, L1
35. Vestergaard M., 2002, ApJ, 571, 733
36. Vernet-Viard, E., Arcidiacono, C., Bagnara, P., et al. 2005, Optical Engineering, 44, 6601